

Vortex dynamics in dilute two-dimensional Josephson junction arrays

Md. Ashrafuzzaman, Massimiliano Capezzali and Hans Beck
Institut de Physique, Université de Neuchâtel, Switzerland

The dynamics of thermally excited vortices in a dilute two-dimensional Josephson junction array where a fraction of the superconducting islands is missing has been investigated using a multiple trapping model. An expression for the frequency dependent mobility of vortices has been calculated which allows to obtain the frequency dependent complex electrodynamic response of the array for different fractions of missing islands.

PACS numbers: 74.50.+r, 74.60.Ge, 05.90.+m

I. INTRODUCTION

Josephson junction arrays (JJA) consist of superconducting islands which are usually arranged on an ordered lattice and coupled by Josephson interaction. Two-dimensional ($2d$) arrays offer a unique opportunity for studying a variety of topics in $2d$ physics, such as phase transitions, non-linear dynamics, percolation, frustration and disorder, in relatively clean experimental realisation. Fabrication of arrays and their basic physical properties have been described in various articles.^{1,2} The islands become superconducting at a given transition temperature T_c^o . Below this temperature each island l is characterized by its superconducting wave function

$$\psi_l = |\psi_l| e^{i\theta_l} \quad (1)$$

with its amplitude and its phase. For all matters and purposes one can assume that $|\psi_l|$ has the same value in each island, such that the phase is the only relevant variable. The islands are linked to each other by the Josephson coupling. The potential energy of the array is then given by

$$H = \sum_{\langle ll' \rangle} J_{ll'} [1 - \cos(\theta_l - \theta_{l'})] \quad (2)$$

The sum can usually be restricted to nearest neighbors in the array and the corresponding Josephson coupling J is related to the critical current I_c by

$$J = \frac{\hbar}{2e} I_c \quad (3)$$

A charging energy required when Cooper pairs move from one island to another has to be added to the expression (2). It is given by a capacitance matrix $C_{ll'}$ coupling the time derivatives of the phases (respectively their conjugate momenta) on different sites.^{1,2,3} Arrays can then be divided into classical and quantum arrays depending on the ratio of the Josephson coupling energy to the relevant charging energy. The experimental work we are referring to in this article has been performed on classical arrays for which charging energies are unimportant. Dynamic phenomena for such arrays are usually described in the framework of the resistively shunted junction (RSJ)

model.^{2,3,4} A resistance matrix $R_{ll'}$ describes the normal currents flowing between the islands.

Research on disordered JJAs is a particularly exciting field. In an array where some sites are missing the electrical and magnetic properties of the lattice may change drastically depending on the number of missing sites relative to the whole array. This effect is related to percolation. About half a century ago this concept was introduced by Flory⁵ and Stockmayer⁶ in order to describe disordered structures. Later on the geometrical and statistical concepts introduced by Broadbent and Hammersley⁷ in connection with the study of diffusion of fluids in random media, introduction of fractal concepts⁸ and the development of computers and simulation techniques as well as theoretical and experimental analysis have contributed to deepening our understanding of the phenomenon of percolation.

We consider an infinite triangular or square lattice, where each site is randomly occupied by a superconducting island with some probability p and empty with probability $1 - p$. The electrical and magnetic properties of the array depend on the value of this percolation fraction p . At a certain value p_c of p the superconducting properties of the array are destroyed. p_c is called critical percolation limit. At high concentration of missing sites, the occupied sites are either isolated or form small clusters of nearest-neighbors, and no path connecting opposite edges of the lattice exists. With increasing p , the mean cluster size of the occupied sites increases up to the appearance of an infinite cluster which connects opposite edges of the whole lattice. The existence of an infinite percolating cluster of occupied sites is connected with the criticality of the percolation (p_c). When p is further increased, more and more sites become part of the infinite cluster of occupied sites, and finally at $p = 1$, all sites belong to the infinite cluster. The percolation threshold depends on different aspects of the lattice structure like its form (triangular, square or others), dimensionality, and on the type of percolation (bond, site, etc.). For example, in a triangular $2d$ array, for site percolation, one can analytically⁹ show that $p_c = 0.5$, but this value can be different for other dimensions of the array and other types of disorder.

Different types of disorder can be considered:

a. For **bond disorder** the parameters characterizing the individual junctions, namely the Josephson couplings J_{ij} , the junction resistances R_{ij} and the mutual capacitances C_{ij} , are random. This type of disorder is realized when the positions of the individual superconducting islands deviate in a random way from their ideal lattice positions or if they have random size, since J_{ij} , R_{ij} and C_{ij} depend on the distance between the adjacent superconductors and on their geometry.

b. For **site disorder** the properties of the superconducting islands, i.e. their resistance and capacitance to ground, are random. More simply, in a dilute array certain islands are totally missing.

Dynamic measurements^{10,11} have been done on dilute, or percolative, arrays for p -values somewhat larger than the percolation threshold $p_c = 0.5$, where the disorder has a marked influence on the properties of the array. At temperatures that are low compared to the Berezinskii-Kosterlitz-Thouless (BKT) transition temperature, T_{BKT} (which in a dilute array is lower than for the regular counterpart, due to the absence of certain bonds, see below) the equations of motion can be linearized, taking into account only small amplitude excitations. The problem at hand is then the same as determining the vibrational modes of a disordered harmonic solid, which is a well studied field.¹² In reference¹³ the impedance $Z(\omega)$ of such a dilute JJA has been determined by evaluating the dynamic voltage correlation function by different methods. The coherent potential approximation (CPA) has proven to be a useful approach for treating dynamic disorder problems. The inverse of the impedance is expressed by an effective coupling function $K(\omega, p)$ depending on frequency and on the dilution fraction p :

$$Z(\omega) = (\eta + \frac{K(\omega, p)}{i\omega})^{-1} \quad (4)$$

corresponding to the effective inductance L and resistance R of the array.

As a main result for the BKT transition these calculations reveal the existence of an effective Josephson coupling constant, J_{eff} . For bonds where one or both of the superconducting islands is missing, the coupling energy vanishes, i.e. $J_{ij} = 0$. Thermodynamics is then governed by an effective coupling constant J_{eff} given by the relation¹³

$$J_{eff} = \frac{p - p_c}{1 - p_c} J \quad (5)$$

and thus the transition temperature T_{BKT} ($k_B T_{BKT} = \frac{\pi}{2} J_{eff}$ or $0.9 J_{eff}$ for triangular or tetragonal array respectively) also decreases.

Close to and above T_{BKT} the dynamic response is then dominated by the motion of thermally created vortices. An equation of motion for vortices can be obtained starting from the RSJ equations for the superconducting phases³. Much analytical and numerical efforts have been devoted³ to describing the dynamic behaviour of

the vortices in regular JJAs. One of the key quantities is the frequency and temperature dependent vortex mobility $\mu(\omega, T)$. For calculating this quantity the Coulomb interaction between the vortices has to be taken into account, which makes the problem difficult.

For disordered JJAs this is an even more complex problem, since one should now describe the motion of interacting particles in a random potential landscape. We will treat the vortex response mainly above T_{BKT} where the interaction between vortices is screened and will thus be neglected. The influence of the random potential on the vortex dynamics will be treated in the Multiple trapping model, that has been developed for handling the motion of electrons in disordered semiconductors. This model will be presented in section II. It allows to calculate the average vortex mobility $\mu(\omega, T)$ in the dilute array as a function of frequency ω and temperature T . In section III the measured electrodynamic response, expressed by the complex impedance of the array, will be related to μ . In section IV our results for μ will be presented and analysed. The main features of our theoretical results for the complex impedance of the array are in good agreement with experimental data¹¹. We shall also show theoretically calculated flux noise spectra for disordered arrays. Finally in chapter V we shall give some conclusions.

II. THE MULTIPLE TRAPPING MODEL

A. The multiple trapping equations

In this chapter we discuss our model for the vortex dynamics in dilute $2d$ JJAs (missing sites or bonds). Deviations from a regular lattice structure will have an influence on the vortices of an array through the Peierls force or pinning potential. The equilibrium arrangement of the (thermal or field induced) vortices and antivortices will correspond to a minimum of the free energy in the given random pinning potential landscape. By thermal excitation, in particular above T_{BKT} , vortices will move around in the dilute array thus giving rise to interesting power law behaviour in the dynamic impedance $Z(\omega)$.¹⁴⁻¹⁶

Our main goal is therefore to calculate the frequency dependent resistance (R) and inductance (L) of a dilute array. In calculating R and L we have to first find the mobility (μ) of the vortex (V) and antivortex (A) in the disordered array. For this we use the so called multiple trapping model (MTM), developed for electronic transport in amorphous semiconductors.¹⁷ In this model the regions where sites of the array are missing are regrouped into holes of different shapes and sizes. The motion of a given particle (we will not distinguish between V and A, since in the absence of interaction they undergo the same influence by the random potential) is then described in probabilistic terms. At a given position \mathbf{r} in the array one can either be in one of the holes of the array or in a regular region, occupied by superconducting islands.

Thus the state of a particle sitting at \mathbf{r} is determined by the following probabilities:

$p(\mathbf{r}, t) \equiv$ probability that a given particle is free at position \mathbf{r} and time t , i.e. it is sitting between holes, in a regular region.

$p_n(t) \equiv$ probability that the particle is trapped in one of the holes which is indexed by n .

In the multiple trapping model the time evolution of these probabilities is governed by two rate equations:

$$\frac{\partial p(\mathbf{r}, t)}{\partial t} + \sum_n \frac{\partial p_n(t)}{\partial t} = -\nabla \cdot \mathbf{j} \quad (6)$$

$$\text{with} \quad \frac{\partial p_n(t)}{\partial t} = -\gamma_{r,n} p_n(t) + \gamma_{t,n} p(\mathbf{r}, t) \quad (7)$$

Here $\gamma_{t,n}$ is the probability per unit time (transition rate) for a particle to get trapped inside the hole n and $\gamma_{r,n}$ is the release rate out of the hole n .

If the particle remains in a regular area it contributes to the current $\mathbf{j} = \mathbf{v}p(\mathbf{r}, t)$ with its velocity $\mathbf{v} = \mu_0 \mathbf{E}$ determined by the mobility μ_0 for a regular array of the same structure, and the effective field \mathbf{E} which will be assumed here as unidirectional (in X direction). Thus the first of the two rate equations can be written as

$$\frac{\partial p(x, t)}{\partial t} + \mu_0 E \frac{\partial p(x, t)}{\partial x} = \sum_n \gamma_{r,n} p_n(t) - \sum_n \gamma_{t,n} p(x, t) \quad (8)$$

Now we use Laplace transformation

$$\hat{f}(z) = \int_0^\infty dt e^{-zt} f(t) \quad (9)$$

$$\frac{\partial f(t)}{\partial t} \rightarrow z \hat{f}(z) - f(0)$$

$f(0)$ being the initial condition.

For (8) this yields

$$z \hat{p}(z) - p(0) + \mu_0 E \frac{\partial \hat{p}(z)}{\partial x} = \sum_n \gamma_{r,n} \hat{p}_n(z) - \sum_n \gamma_{t,n} \hat{p}(z) \quad (10)$$

and for (7)

$$z \hat{p}_n(z) = \gamma_{t,n} \hat{p}(z) - \gamma_{r,n} \hat{p}_n(z) + p_n(0) \quad (11)$$

Imposing the initial condition $p(0) = 1$ and $p_n(0) = 0$ we get from the previous equation

$$\hat{p}_n(z) = \frac{\gamma_{t,n}}{z + \gamma_{r,n}} \hat{p}(z) \quad (12)$$

Now we define

$$\pi_n(z) = \frac{\gamma_{t,n}}{z + \gamma_{r,n}} \quad (13)$$

and equation (10) becomes

$$z \hat{p}(z) (1 + \pi(z)) = 1 - \mu_0 E \frac{\partial \hat{p}(z)}{\partial x} \quad (14)$$

The quantity

$$\pi(z) = \sum_n \pi_n(z) \quad (15)$$

will turn out to play a central part for the frequency and temperature dependence of the electrodynamic response of the array.

In order to get concrete expressions for our transition rates we consider thermal equilibrium in zero external field where the probabilities, $p(\mathbf{r}, t) = p_0$ and $p_n(t) = p_n$, are independent of space and time. The former is simply proportional to the total regular area $p_0(La)^2$, a being the lattice constant, L^2 the total number of sites :

$$p_0 = A p_0 (La)^2 \quad (16)$$

The probabilities p_n are given by a Boltzmann factor, involving the binding energy E_n of a particle trapped in hole number n , and the surface S_n of the corresponding hole

$$p_n = A S_n e^{\beta E_n} \quad (17)$$

The thermally activated release rate is given by

$$\gamma_{r,n} \doteq r e^{-\beta E_n} \quad (18)$$

with r being the attempt frequency and $\beta = \frac{1}{k_B T}$.

In the case of detailed balance all terms in equation (7) vanish, therefore

$$p_0 \gamma_{t,n} = p_n \gamma_{r,n} \quad (19)$$

and $\gamma_{t,n} = \frac{p_n}{p_0} \gamma_{r,n} = r \frac{S_n}{p(La)^2}$.

For the circular holes, considered here, the area is given by $S_n = S(N) = N a^2$, N being the number of missing sites.

Combining these relations we find the following expression for the trapping rate $\gamma_{t,n} = \gamma_t(N)$

$$\gamma_t(N) = r \frac{N}{p L^2} = r \frac{N}{p N_{tot}} \quad (20)$$

where $N_{tot} = L^2 \equiv$ is the total number of sites.

B. The vortex mobility

The mean velocity \bar{v} of a V is related to its mean position \bar{x} by

$$\bar{v} = \frac{\partial \bar{x}}{\partial t} = \int d^2 r x \frac{\partial p(\mathbf{r}, t)}{\partial t} \quad (21)$$

Through Laplace transformation (9) we get

$$\hat{v} = z \hat{x} = \int d^2 r x z \hat{p}(\mathbf{r}, z) \quad (22)$$

taking, for simplicity, $\bar{x}(0) = 0$, i.e. the vortex started ($t = 0$) its motion from the origin of the lattice. Now using equation (14) the previous equation, through partial integration, becomes

$$\begin{aligned}\hat{v} &= \int d^2rx \frac{1 - \mu_0 E \frac{\partial \hat{p}(\mathbf{r}, z)}{\partial x}}{1 + \pi(z)} \\ &= \frac{-\mu_0 E}{1 + \pi(z)} \int d^2rx \frac{\partial \hat{p}(\mathbf{r}, z)}{\partial x} + \int d^2r \frac{x}{1 + \pi(z)} \\ &= \frac{\mu_0 E}{1 + \pi(z)}\end{aligned}\quad (23)$$

The last term of the first part in the previous equation represents the initial condition of the velocity and contributes zero by our assumption.

The effective mobility μ of a V is given by $\hat{v} = \mu E$. We get from the previous equation¹⁸

$$\mu(z) = \frac{\mu_0}{1 + \pi(z)}\quad (24)$$

and $\pi(z)$ is given by equation (15). The purpose of our calculations is to exhibit, through the mobility μ , the influence of disorder on the dynamic response of the vortex system. In order not to mix these effects with the intrinsic frequency dependence of μ in regular arrays and for computational simplicity we take μ_0 , the vortex mobility in the regular array, to be constant, giving the scale unit for μ (see expression (38)).

Taking $D(N)$ to be the number of holes having N missing sites and considering (20) for $\gamma_t(N)$, the key quantity $\pi(z = i\Omega)$, for real frequencies Ω , can be expressed by

$$\begin{aligned}\pi(z = i\Omega) &\equiv \pi(\Omega) \rightarrow \sum_N D(N) \pi(z = i\Omega, N) \\ &= \sum_N \gamma_t(N) \frac{D(N)}{i\Omega + r e^{-\beta E(N)}} \\ &= \int_1^{N_{max}} dN \frac{\hat{D}(N) N}{i \frac{\Omega}{r} + e^{-\beta E(N)}}\end{aligned}\quad (25a)$$

In the above expression, $\hat{D}(N) = \frac{D(N)}{p N_{tot}}$ is a normalized number density of holes. We introduce the dimensionless frequency $\omega = \frac{\Omega}{\omega_a}$, with $\omega_a = \frac{k_B T_{BKT} \mu_0}{a^2}$ being a characteristic frequency which includes the lattice constant a of the array and the bare vortex mobility μ_0 of the ordered array. Introducing the vortex diffusion constant by $D_0 \equiv k_B T_{BKT} \mu_0$, for temperature T_{BKT} , the frequency ω_a is given by $\omega_a = \frac{D_0}{a^2}$. Its inverse is thus the average time for a vortex to diffuse across one lattice constant a . A very sensitive step in our entire procedure is represented by the choice of the attempt frequency r . We will write the latter as $r = \omega_a f(t)$ where $t = \frac{T}{T_{BKT}}$ represents the scaled temperature. Here we consider either $f(t) = t$, if the attempt frequency is considered to increase with temperature - i.e. $r = \omega_a t$ -, or $f(t) = 1$, in the case where r is assumed to be constant. At first glance, the former case probably appears to be more sound and intuitive from a physical point of view. However, choosing

a constant r may be understood as arising from the fact that our system is considered to be overdamped; hence, kinetic energy - which is indeed proportional to temperature - is an ill-defined quantity and one may consequently be led to assume, that r does not depend on temperature and simply represents a characteristic frequency of the vortex system. We end up with

$$\pi(\omega) = \int_1^{N_{max}} dN \frac{\hat{D}(N) N}{i \frac{\omega}{f(t)} + e^{-\beta E(N)}}\quad (25b)$$

The value of N_{max} has to guarantee the correct total number of missing sites:

$$N_{tot}(1 - p) = \sum_1^{N_{max}} D(N) N\quad (26)$$

Therefore N_{max} depends on the value of p , the sample size N_{tot} and of course on the choice of a hole distribution function $D(N)$.

C. Binding energy for circular holes

The energy of a phase configuration is expressed by (2). In the case of percolative arrays

$$J_{ll'} = \begin{cases} J & \text{with probability } p \\ 0 & \text{with probability } 1 - p \end{cases}\quad (27)$$

where J is the Josephson coupling constant between two islands.

Now when phase field $\theta(r)$ varies slowly we can write $1 - \cos(\theta_l - \theta_{l'}) \approx \frac{(\theta_l - \theta_{l'})^2}{2}$, so we get, converting summation into integration for slowly varying phase fields,

$$E \approx J \int d^2r \frac{(\nabla \theta)^2}{2}\quad (28)$$

For a vortex at the origin, the phase field is given by $\theta(r) = \arctan \frac{y}{x}$ where x and y are cartesian coordinates in the array. We get $|\nabla \theta|^2 = \frac{1}{r^2}$ and the total energy of a vortex in the array is

$$E_V = \frac{J}{2} \int_{r_1}^L d^2r \frac{1}{r^2}\quad (29)$$

where L is the size of array and r_1 is a lower cut-off corresponding to lattice constant. Now the binding energy of the V or A inside a hole (approximated to be circular) of radius r_2 with $\pi r_2^2 = (N + 1) \pi r_1^2$ (the area of the hole is equal to $N + 1$ times the area of a unit cell) is

$$\begin{aligned}E(N) &= \frac{J}{2} \int_{r_1}^L d^2r \frac{1}{r^2} - \frac{J}{2} \int_{r_2}^L d^2r \frac{1}{r^2} \\ &= \frac{J}{2} \int_{r_1}^L dr r \frac{1}{r^2} \int_0^{2\pi} d\theta - \frac{J}{2} \int_{r_2}^L dr r \frac{1}{r^2} \int_0^{2\pi} d\theta \\ &= \pi J \ln \frac{r_2}{r_1} = \pi J \ln \sqrt{N + 1}\end{aligned}\quad (30)$$

because $\pi(r_2^2 - r_1^2) = N\pi r_1^2$ or $\frac{r_2}{r_1} = \sqrt{N+1}$.

Using (5)

$$k_B T_{BKT} = \frac{\pi}{2} J_{eff} = \frac{\pi}{2} \frac{p - p_c}{1 - p_c} J \quad (31)$$

the exponent of the Boltzmann factor in (25) can be rewritten as

$$\beta E(N) = \frac{1 - p_c}{p - p_c} \frac{2}{t} \ln \sqrt{N+1} \quad (32)$$

Thus we obtain from equation (25)

$$\pi(\omega) = \frac{1}{N_{tot} p} \int_1^{N_{max}} dN \frac{ND(N)}{i\frac{\omega}{t} + (1+N)^{-a(t)}} \quad (33)$$

with a temperature dependent exponent

$$a(t) = \frac{1}{t} \frac{1 - p_c}{p - p_c} \quad (34)$$

III. ELECTRODYNAMIC RESPONSE OF THE ARRAY

A. Resistance and Inductance

Generally, the response of the array to an external electromagnetic excitation can be characterized taking the contributions of the superfluid, normal electrons and vortices into account. This corresponds to a two-fluid model, where the medium is described by an inductive superfluid channel in parallel with a dissipative channel.

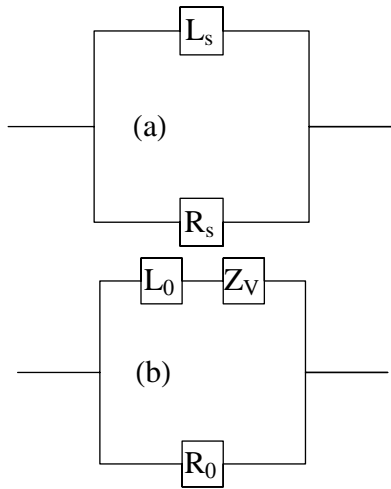


FIG. 1: Circuit diagram for a 2d superconductor. (a) in terms of an inductive and resistive component, (b) in the presence of vortices.

The measured quantity in the array is the sheet conductance G . The effect due to the vortices can be incorporated in this conductance of the array. In the presence of a current, the vortices experience a Lorentz force which will set them in motion perpendicular to the current flow. Associated with the vortex motion, there is an electric field which adds to the electric field of the accelerated superfluid background. This phenomenon therefore leads to an increase in the sheet impedance by an amount Z_V , which comes in series with the impedance of the superfluid background, as shown in figures 1(a) and 1(b) schematically.

G is the sheet conductance which is the inverse of the sheet impedance Z

$$\begin{aligned} G &= \frac{1}{R_s} + \frac{1}{i\Omega L_s} = Z^{-1} \\ &= \frac{1}{R_0} + G_{sup} \end{aligned} \quad (35)$$

where G_{sup} is the superconducting part of the conductance, the resistance R_0 is due to the dissipative processes (Ohmic contribution of the conductance) resulting from the currents flowing in the junction in the absence of vortices and antivortices, whereas L_s is the sheet inductance and R_s is the sheet resistance when there are vortices and antivortices present in the array.

We shall now relate the resistive (R_s) and inductive (L_s) parts of the sheet conductance G with the resistive (R_V) and inductive (L_V) parts of the vortex impedance Z_V through the following relations: $Z_V = Z_{sup} - i\Omega L_0 = G_{sup}^{-1} - i\Omega L_0$ and $G_{sup} = G - \frac{1}{R_0} = \frac{1}{R_s} - \frac{1}{R_0} + \frac{1}{i\Omega L_s}$ so $Z_V = \frac{1}{R_s^{-1} - R_0^{-1} + (i\Omega L_s)^{-1}} - i\Omega L_0 = R_V + i\Omega L_V$ which gives

$$R_V = \frac{R_s^{-1} - R_0^{-1}}{(R_s^{-1} - R_0^{-1})^2 + (\Omega L_s)^{-2}} \quad (36)$$

$$L_V = \frac{1}{\Omega} \frac{(\Omega L_s)^{-1}}{(R_s^{-1} - R_0^{-1})^2 + (\Omega L_s)^{-2}} - L_0 \quad (37)$$

Here L_0 , the inductive part, arises from the currents flowing in the junction in absence of vortices and antivortices.

The frequency dependent dielectric function of the vortex system $\epsilon_V(\Omega) = 1 - iZ_V/(\Omega L_0)$ is related to the vortex mobility $\mu(\Omega)$ by the following expression

$$\begin{aligned} i\Omega L_0 \epsilon_V(\Omega) &= i\Omega L_0 \left(1 + 2\pi q_0^2 n \mu(\Omega) \frac{1}{i\Omega}\right) \\ &= i\Omega L_0 + L_0 2\pi q_0^2 n \mu_0 (\nu'(\Omega) + i\nu''(\Omega)) \\ &= i\Omega L_0 + Z_V = i\Omega L_0 + R_V + i\Omega L_V \end{aligned} \quad (38)$$

where q_0 ($q_0^2 = 2\pi J$) is the charge of a vortex, n is the vortex density and $\nu(\Omega) = \frac{\mu(\Omega)}{\mu_0} = \nu'(\Omega) + i\nu''(\Omega)$ is our dimensionless mobility.

Solving for the real and imaginary parts from the previous equation through the use of equation (5) for the

triangular array we get

$$R_V = 2\pi q_0^2 n \mu_0 \nu' L_0 = 8\pi \omega_a L_0 \frac{1-p_c}{p-p_c} \bar{n} \nu'(\omega) \quad (39)$$

$$L_V = 2\pi q_0^2 n \mu_0 \frac{\nu''}{\Omega} L_0 = 8\pi L_0 \frac{1-p_c}{p-p_c} \bar{n} \frac{\nu''(\omega)}{\omega} \quad (40)$$

where we have used $\bar{n} = na^2$ which is the density of V per unit cell.

As $Z_V + i\Omega L_0 = i\Omega L_0 + 2\pi q_0^2 n L_0 \mu_0 (\nu'(\Omega) + i\nu''(\Omega))$ we get

$$\begin{aligned} \frac{1}{R_s} - \frac{1}{R_0} + \frac{1}{i\Omega L_s} &= \frac{1}{Z_V + i\Omega L_0} \\ &= \frac{1}{L_0 i(\Omega + 2\pi q_0^2 n \mu_0 \nu''(\Omega)) + 2\pi q_0^2 n \mu_0 \nu'(\Omega)} \\ &= \frac{1}{L_0} \frac{\sigma'_V - i(\Omega + \sigma''_V)}{(\Omega + \sigma''_V)^2 + \sigma_V'^2} \end{aligned} \quad (41)$$

where we have used

$$\begin{aligned} \sigma'_V &= 2\pi q_0^2 n \mu_0 \nu'(\Omega) = (2\pi)^2 J n \mu_0 \nu'(\Omega) \\ &= 8\pi \omega_a \bar{n} \frac{1-p_c}{p-p_c} \nu'(\Omega) \end{aligned} \quad (42)$$

$$\begin{aligned} \sigma''_V &= 2\pi q_0^2 n \mu_0 \nu''(\Omega) = (2\pi)^2 J n \mu_0 \nu''(\Omega) \\ &= 8\pi \omega_a \bar{n} \frac{1-p_c}{p-p_c} \nu''(\Omega) \end{aligned} \quad (43)$$

where σ'_V and σ''_V are the real and imaginary parts of the vortex conductance σ_V which is related to vortex dielectric function through $\epsilon_V(\Omega) = 1 + \frac{\sigma_V(\Omega)}{i\Omega}$.

Separating the real and imaginary parts from both sides of equation (41) we get¹⁸

$$\begin{aligned} \frac{1}{R_s} - \frac{1}{R_0} &= \frac{\sigma'_V}{L_0((\Omega + \sigma''_V)^2 + \sigma_V'^2)} \\ &= \frac{8\pi}{L_0 \omega_a} \frac{\frac{1-p_c}{p-p_c} \bar{n} \nu'(\omega)}{(\omega + 8\pi \frac{1-p_c}{p-p_c} \bar{n} \nu''(\omega))^2 + (8\pi \frac{1-p_c}{p-p_c} \bar{n} \nu'(\omega))^2} \end{aligned} \quad (44)$$

$$\begin{aligned} \frac{1}{L_s} &= \frac{1}{L_0} \frac{\Omega(\Omega + \sigma''_V)}{(\Omega + \sigma''_V)^2 + \sigma_V'^2} \\ &= \frac{1}{L_0} \frac{\omega(\omega + 8\pi \frac{1-p_c}{p-p_c} \bar{n} \nu''(\omega))}{(\omega + 8\pi \frac{1-p_c}{p-p_c} \bar{n} \nu''(\omega))^2 + (8\pi \frac{1-p_c}{p-p_c} \bar{n} \nu'(\omega))^2} \end{aligned} \quad (45)$$

The scale quantity R_0 is expressed by

$$R_0 = 4.5 R_J \quad (46)$$

where R_J is the junction resistance and the prefactor 4.5 is an estimate deduced by setting the energy barrier for vortex motion to its theoretical value (for details see ref.¹¹).

The temperature dependent expression for L_0 , the sheet inductance of a single junction, is given by (for details see ref.¹¹)

$$\frac{1}{L_0(T)} = \sqrt{3} \frac{2e}{\hbar} b^{-\zeta} I_c \left(1 - \frac{T}{T_c}\right)^2 e^{-c\sqrt{T}} \quad (47)$$

Here ζ is a critical exponent in two dimensions, $b^{-\zeta}$ is some constant deduced experimentally by setting the energy barrier for vortex motion to its theoretical value¹⁰, I_c is the critical current of a single junction, c is some constant in unit of $K^{-1/2}$ and T_c is the transition temperature for the superconducting islands.

B. Flux noise

Flux noise measurements give interesting information about time correlations in the vortex dynamics. The Fourier transform $S_\phi(\omega)$ of the dynamic correlation function of the magnetic flux threading through a closed loop above the array is given by³

$$S_\phi(\omega) = S_0 \int_0^\infty dk \frac{J_1(kR)^2 e^{-2kd}}{k(1+\lambda k)^2} \text{Re}[\phi_{\rho\rho}(k, -i\omega)] \quad (48)$$

where $J_1(x)$ is the first order Bessel function and λ represents the magnetic penetration depth of the JJA and $\phi(k, z)$ is the Fourier-Laplace transform of the dynamic correlator of the vortex charge density $\rho_V(r, t)$

$$\phi(k, z) = \int d^2r \int_0^\infty dt e^{-zt} e^{i\mathbf{k}\cdot\mathbf{r}} \langle \rho_V(\mathbf{r}, t) \rho_V(\mathbf{0}, 0) \rangle \quad (49)$$

It can be evaluated, for example, by Mori's procedure for calculating dynamic correlation functions, which yields the following form

$$\phi(k, z) = \frac{S(k)}{z + \frac{k_B T k^2 \mu(z)}{S(k)}} \quad (50)$$

involving the static charge structure factor $S(k)$ and the dynamic vortex mobility $\mu(z)$. Neglecting again the effect of vortex interaction we use the mobility resulting from the multiple trapping model for the flux noise calculation. The structure factor should, in principle, be calculated by taking into account the effect of the random potential landscape due to the holes on the vortex configuration. We instead take the simple form¹⁹

$$S(k) = \frac{k^2}{k^2 + k_0^2} \quad (51)$$

with

$$k_0^2 = \frac{2\pi q_0^2 n}{k_B T} \quad (52)$$

which has the correct behaviour for $k \rightarrow 0$ (charge neutrality of the V-A-system) and for $k \rightarrow \infty$.

IV. RESULTS

In this chapter we present our theoretical results for the frequency dependent mobility of vortices or antivortices in a dilute superconducting array using the multiple trapping model, the conductance of the array and the vortex resistance. Affolter¹¹ has measured the properties of such a disordered array near the critical percolation limit p_c below which the superconductivity of the array destroys (a publication of his results is in preparation).

In order to compare our theoretical results with these experimental data we have to determine the values of the parameters characterizing the array.

The measurements¹¹ have been performed on a triangular JJA of lead islands at $p = 0.515$ with the following characteristics: $R_J \approx 5.2m\Omega$, $\zeta \approx 1$, $a \approx 15 \times 10^{-6}m$, $I_c(0) \approx 14mA$, $c \approx 3K^{1/2}$, $T_c^o = 7K$, $T_{BKT} = 3.7K$, $b \approx 0.22$. From this we find: $D_0 \approx 2 \times 10^{-5} \frac{m^2}{s}$ and $\omega_a \approx 10^6 \text{Hz}$.

An important goal consists in elucidating the way in which the disorder of the dilute array influences vortex motion. The key quantity for this is $\pi(\omega)$ given by expression (33). Given the limits of the integral over N three frequency regimes can be distinguished, namely

$$\begin{aligned} (a) \quad \omega < \omega_1 &\equiv (1 + N_{max})^{-a(t)} \\ (b) \quad \omega > \omega_2 &\equiv 2^{-a(t)} \\ (c) \quad \omega_1 < \omega < \omega_2 \end{aligned} \quad (53)$$

In regions a and b the frequency dependence of the real and imaginary parts, $\pi'(\omega)$ and $\pi''(\omega)$, does not depend on the details of the hole distribution $D(N)$. It is given by

$$\begin{aligned} \text{Region } a : \quad \pi'(\omega) &= \pi_0, \quad \pi''(\omega) \propto \omega \\ \text{Region } b : \quad \pi'(\omega) &\propto \frac{1}{\omega^2}, \quad \pi''(\omega) \propto \frac{1}{\omega} \end{aligned} \quad (54)$$

In the intermediate region, however, the form of $D(N)$ will be reflected in temperature dependent frequency exponents for $\pi'(\omega)$ and $\pi''(\omega)$. A simple estimate can be made by assuming a power law distribution of hole sizes:

$$D(N) = D_0 N^{-s} \quad (55)$$

which turns out to correspond quantitatively with the arrays, studied in Ref.¹¹, where $s \approx 1.8$. For frequencies lying well inside the interval $[\omega_1, \omega_2]$ the power law of π can be simply calculated:

$$\pi(\omega) \propto \int_1^{N_{max}} dN \frac{ND(N)}{i\omega + (1+N)^{-a(t)}} \approx I_0(i\omega)^{-u(t)} \quad (56)$$

$$I_0 = \int_0^\infty dy \frac{y^{1-s}}{1+y^{-a}} \quad (57)$$

$$u = 1 + \frac{2-s}{a} \quad (58)$$

t	$a(t)$	ω_1	ω_2	$u(t)(s=1.8)$	$u(t)(s=0.3)$
0.9	37	10^{-53}	$7 \cdot 10^{-12}$	1	1.05
2	17	$9 \cdot 10^{-25}$	$8 \cdot 10^{-6}$	1.01	1.1
6	5.5	$2 \cdot 10^{-8}$	0.02	1.04	1.3
10	3.3	$2 \cdot 10^{-5}$	0.1	1.06	1.5

TABLE I: Some parameters for $p = 0.515$ and $N_{max} = 25$; $a(t) = \frac{1}{t} \frac{1-p_c}{p-p_c} = \frac{1}{t} \frac{0.5}{0.015} = \frac{33}{t}$, $\omega_1 = (1+25)^{-a}$ and $\omega_2 = (1+1)^{-a}$.

We summarize in Table I the values of ω_1 , ω_2 and u using the parameters corresponding to the experimental data of Ref.11, namely $p = 0.515$, $0.9 < t < 10$ and $N_{max} = 25$. For the given parameter values it turns out that the exponent $u \approx 1$ is almost T -independent. The resulting frequency dependence the real part of π , $\pi' \sim 1/\omega$, is unusual, since one expects π' to be an even function of ω , as it is indeed the case in regions a and b , see relations (54). The power law behaviour ($\pi \sim \omega^{-u}$) is the result of the integration over a continuous spectrum of relaxation rates in (56). For comparison we give another form of $D(N)$ which gives more weight to large holes ($s = 0.3$). The corresponding exponent has a more pronounced T -dependence.

The vortex mobility resulting from π through (24) will determine the electrodynamic response in (44) and (45), as well as flux noise (48). Its behaviour, in units of the free vortex mobility μ_0 , is shown in figure 2 for different temperatures and for different defect concentrations $1-p$. The three frequency regimes are again visible, although the curves have more structure than the ones for π since $\pi'(\omega)$ and $\pi''(\omega)$ are combined with each other in the expression (24) for $\nu'(\omega)$ and $\nu''(\omega)$.

At very high frequencies, namely $\omega > 1$ the real part of the mobility is constant with the bare value μ_0 . In this regime we are investigating the short-time response of the array: the vortices lying outside the holes do not have a significant probability of being trapped and their mobility is just the bare one. At the other extremity of the frequency spectrum, the vortex mobility is also constant but the bare value μ_0 is renormalized by $1 + \pi_0$ leading to a reduction by several orders of magnitudes, strongly depending on p . Over very long time spans the vortices get trapped and released many times and, as they do not contribute to mobility as long as they stay in a hole, the overall mobility dramatically diminishes upon increasing the number and size of the holes.

The imaginary part of the vortex mobility displays a maximum near $\omega = 1$. For lower frequencies $Im[\mu(\omega)] \propto \omega$, although at $p = 0.6$ and below T_{BKT} a small kink appears around $\omega \sim 10^{-7}$ (especially for $s = 0.3$).

The intermediate-frequency behaviour of the real part of the vortex mobility can be understood by looking care-

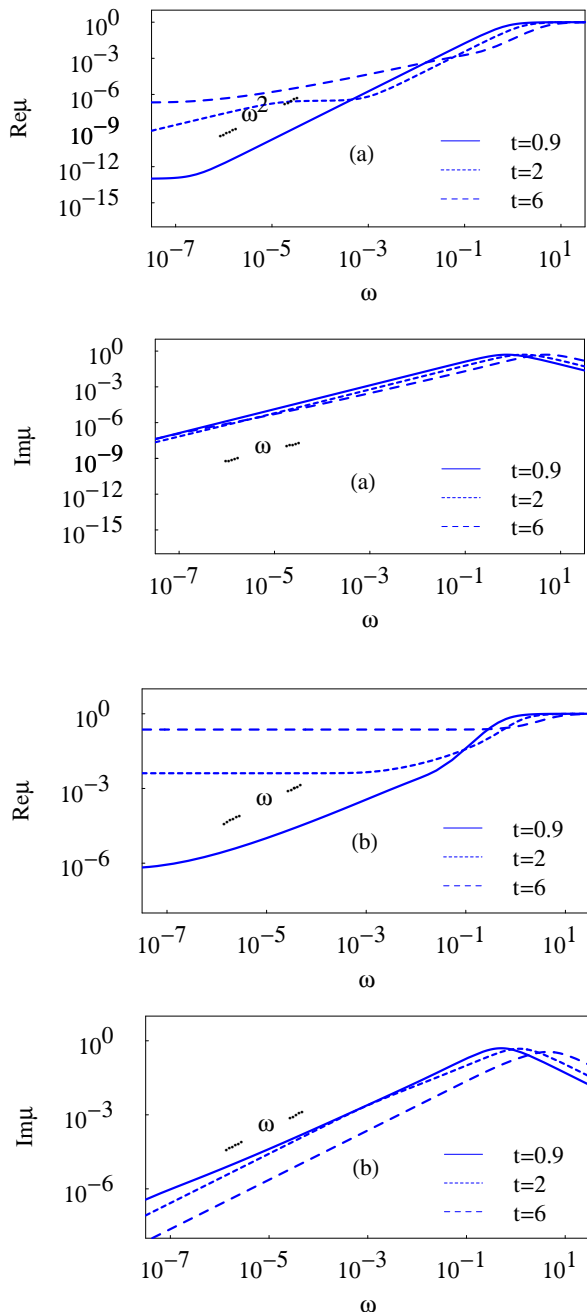


FIG. 2: μ vs ω for (a) $p = 0.515$ ($N_{max} = 25$) and for (b) $p = 0.6$ ($N_{max} = 22$). $s = 1.8$. In order to see the frequency dependence easily the slopes for ω , respectively ω^2 , are given.

fully at the interplay of the real and imaginary parts of $\pi(\omega)$ going into $\mu'(\omega) = \frac{1+\pi'(\omega)}{(1+\pi'(\omega)^2)+\pi''(\omega)^2}$.

Two frequency domains show up: In a range below $\omega = 1$, extending as far down as 10^{-7} for $t = 0.9$, $\pi''(\omega) \propto \omega^{-1}$ for all interesting frequencies, while $\pi'(\omega)$

becomes significantly lower than unity. Thus the real part of the mobility increases quadratically with frequency, which is in some sense a surprisingly normal behaviour. Conversely, at smaller frequencies, $\pi'(\omega)$ becomes constant, while $\pi''(\omega) \propto \omega$ (i.e. it reaches a maximum at some frequency, below the quadratic-behaviour window), giving rise to a constant vortex mobility with a value intermediate between μ_0 and the low frequency limit. The two frequency regimes get shifted towards lower ω -values when temperature is reduced, as it can be seen in figure 2. The curves in figure 2 have been calculated for the choice $f(t) = t$ in equation (25b). We have verified that the result for $f(t) = 1$ is almost identical.

In addition to the intermediate-frequency regime, where the real part of the mobility becomes constant, we see on Fig. 2, that at $t = 2$ yet another anomalous regime shows up at very low frequencies, where $\mu'(\omega) \propto \omega$, approximately. At high temperature ($t = 6$) and at frequencies below the tiny $\mu \propto \omega^2$ window centered around $\omega \approx 1$, the mobility plateau gets replaced by a regime where $\mu'(\omega) \propto \omega^{0.8}$, down to $\omega \approx 10^{-6}$. The non-integer exponent arises from the fact that, in accordance with the Table I, $\pi''(\omega) \propto \omega^{-1.04}$ in this frequency window, while $\pi'(\omega) \propto \omega^{-1}$ and $\pi'(\omega) \gg 1$ still. Obviously, this non-integer power-law behaviour of the real part of the mobility also arises at lower temperatures, but it becomes less pronounced as the exponent $u(T)$ is extremely close to unity at $t = 2$. In order to confirm this behaviour, we have computed the vortex mobility at $s = 0.3$, a choice for which the exponent $u(T)$ has a much more marked temperature-dependence than at $s = 1.8$. see Table I. In the former case, we find that, at $t = 0.9$, no relevant changes occur, with respect to the results obtained at $s = 1.8$. Nevertheless, at higher temperature $t = 2$, the intermediate-frequency plateau discussed above gets substantially reduced and covers at most only one frequency decade. At even higher temperature $t = 6$, the plateau is replaced by an anomalous regime extending roughly from $\omega \approx 10^{-7}$ to $\omega \approx 10^{-2}$, in which the real part of the mobility behaves as a power-law $\omega \propto \omega^{-0.7}$ again with a non integer exponent. For both choices of the parameter s , the real part of the mobility eventually turns to a constant at extremely low frequencies. Therefore, in conclusion, for temperatures above T_{BKT} , the mobility displays four distinct frequency regimes, which collapse into three regimes below the transition temperature.

We now turn to the electrodynamic response for which experimental data are available in ref.¹¹. For the vortex density n showing up in (44) and (45) we have used the values obtained in the references^{20,21} through Monte Carlo simulations of the regular arrays. In order to have a consistent treatment one should, of course, know the vortex density of a dilute array. The presence of holes indeed makes the formation of phase singularities more easy, since, in particular, vortices centered in a hole cost less energy than in a regular array. However, for temperatures above T_{BKT} , where even in a regular array the number of vortices grows rather rapidly, the difference

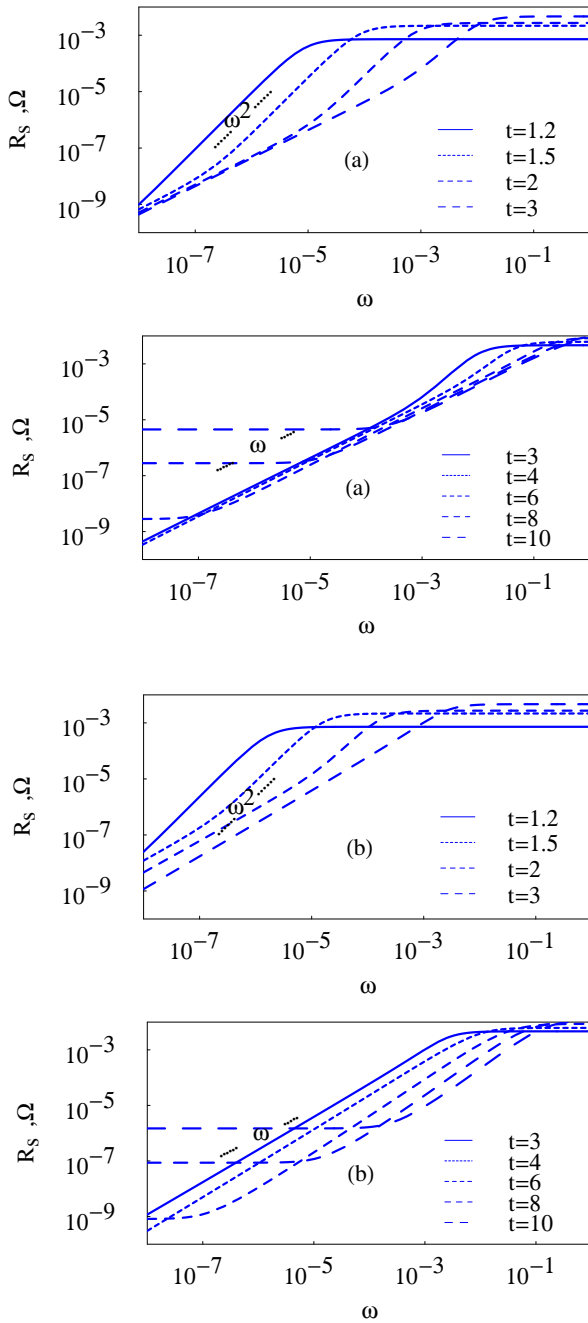


FIG. 3: R_s vs ω for $p = 0.515$. (a) $s = 1.8$ and (b) $s = 0.3$.

should not be too important. Our sheet resistance curves for $p = 0.515$ are shown in figures 3(a) and 3(b) for two different exponents s in $D(N)$, see equation (55). For the sake of comparison figure 4 shows the same curves for a slightly larger value of p . The following observations can be made:

- The same three frequency regimes determining the quantity $\pi(\omega)$ and the vortex mobility can be identi-

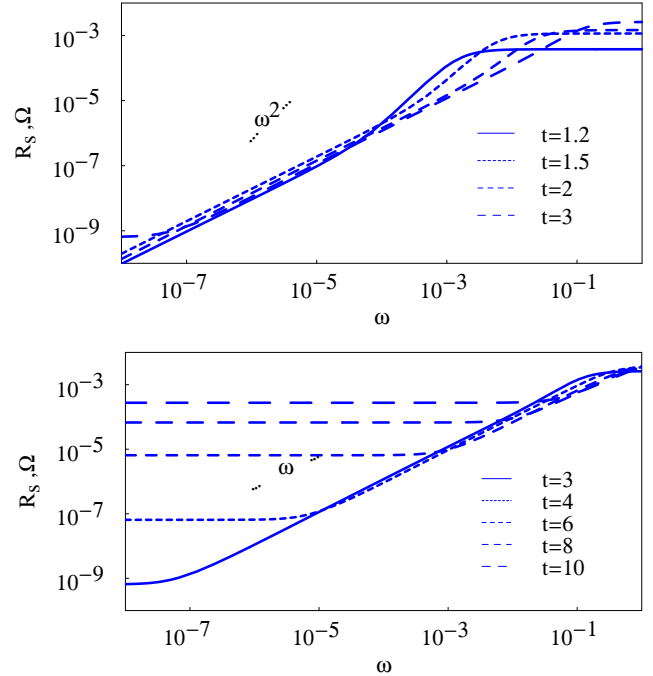


FIG. 4: R_s vs ω plot for $p = 0.53$ ($N_{max} = 25$) and $s = 1.8$.

fied in $R_s(\omega)$: at very low and at very high frequencies R_s is constant, whereas in the intermediate regime it increases as a power of ω : $R_s \sim \omega^{x(T)}$. This temperature dependent exponent x is a fine detail of the MT model which is in good agreement with the experimental data. For higher temperature $x = 1$, which is again an interesting signature of the disorder of the array. For lower T the sheet resistance undergoes an upturn to ω^2 -behaviour, which is clearly visible in Fig. 3. The latter behaviour is intimately linked to the real part of the vortex mobility (discussed above) going through an intermediate plateau in some frequency window. Indeed, within the latter, we notice that $\mu'_V(\omega) \ll \mu''_V(\omega)$, trivially implying $\sigma'_V(\omega) \ll \sigma''_V(\omega)$. Upon considering Eqns. (42) and (43) for p close to p_c , we furthermore deduce that $\sigma''_V(\omega)$ is larger than frequency in the "plateau" ω -window. Consequently, inserting this into expression (44), we obtain $R_s^{-1} = \frac{L_0 \sigma''_V(\omega)^2 + R_0 \sigma'_V(\omega)}{R_0 L_0 \sigma''_V(\omega)^2}$. Hence, bearing in mind that for all the frequencies that we are considering here, $\mu''_V(\omega) \propto \omega$, there exists a frequency window in which $\mu'_V(\omega) = const.$ implies $R_s \propto \omega^2$, especially for temperatures close to and above T_{BKT} , where $L_0(T)$ is small. In turn, at higher frequencies, we fall in the ω -window where $\mu'_V(\omega) \propto \omega^2$, in which the sheet resistance turns to a constant. In conclusion, the anomalous vortex mobility plateau which arises from the balance between the real and imaginary parts of $\pi(\omega)$ is at the root of the ω^2 -upturn of the sheet resistance in our model.

- In experiment R_s approaches a square root frequency dependence for ω larger than ω_c (see ref.¹¹), rather than

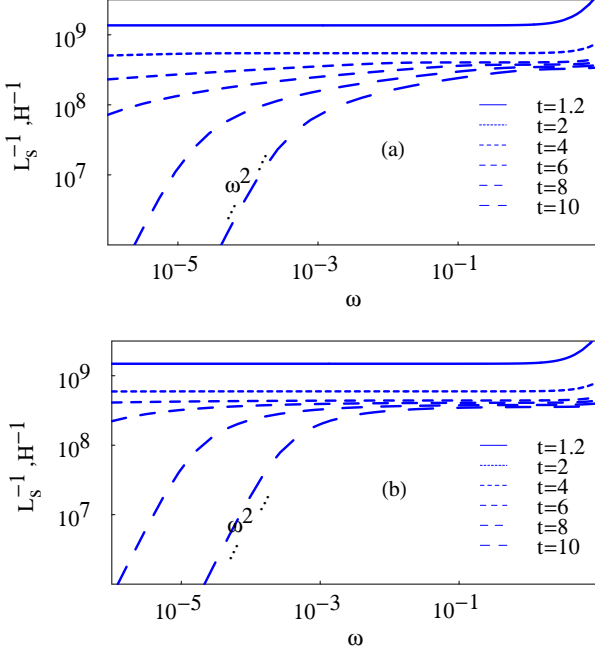


FIG. 5: L_s vs ω plot for $p = 0.515$. (a) $s = 1.8$, (b) $s = 0.3$.

becoming constant. This may point to a new dynamic regime that is not fully covered by our model calculations. There is however a growing tendency in the Theoretical curves to such a further increase of R_s at the highest frequencies shown for larger p -values (see figure 4).

- The temperature variation of the slow frequency level of R_s , as well as the difference between the low and high frequency limits are larger in the MTM results than in experiment. This may be a hint that the model, at least for the p -value used, attributes too much value to the disorder of the array.

- For higher temperatures the measured data show universality: when the curves have reached a linear slope they lie on top of each other. In the model results this universality is rather well reproduced for a higher value of the exponent s of the hole distribution function $D(N)$ (figures 3(a) and 4), which corresponds to the effective hole hierarchy of the experimental array¹¹, giving thus less weight to large holes than the lower values of s .

The inverse of the inductive response, $1/L_s$, for our MTM is presented in figures 5(a) and 5(b) for the same parameters as in figure 3 for R_s and for a large p in figure 6. Comparing the two leads to the following observations:

- The three frequency regimes are again visible: for small and for large ω $1/L_s$ varies as ω^2 , whereas in-between it is constant. The experimental data¹¹ show this behaviour for low frequency. However, except for the lowest temperature, there is no real constant part, but relatively smooth cross-over to a square root like behaviour when ω increases. This again points to a high

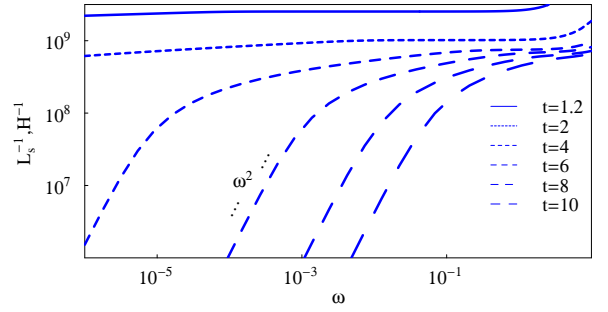


FIG. 6: L_s vs ω plot for $p = 0.53$. $s = 1.8$.

frequency dynamics that is not covered by our MT model for $p = 0.515$. However, the experimentally obtained $\sqrt{\omega}$ type behaviour is almost achieved in our theoretical model for higher values of p and T .

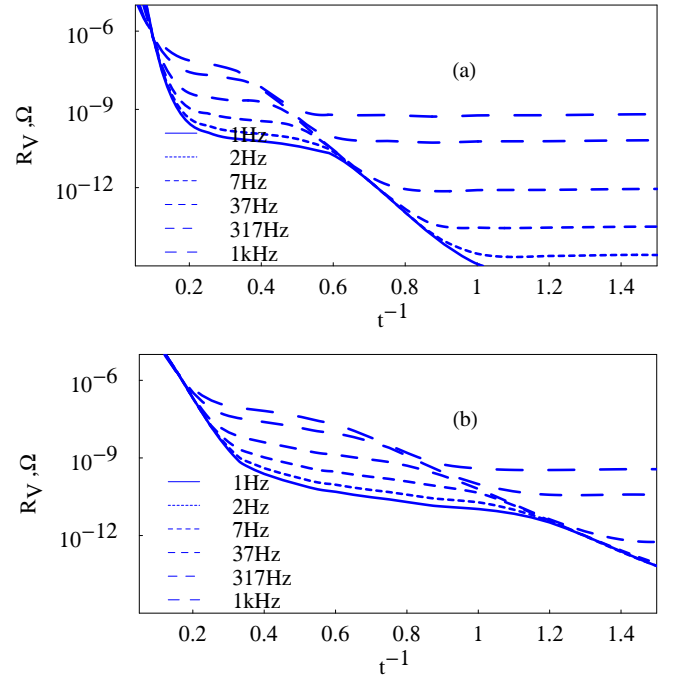


FIG. 7: R_V vs $1/t$ for different Ω . (a) for $p = 0.515$, (b) for $p = 0.53$. $s = 1.8$.

On the whole our MTM results are in good agreement with the measured data. Certain experimental features (in particular the low frequency and low temperature behaviour of R_s) are better reproduced for the value $p = 0.515$ of the percolation parameter, which corresponds to the experimental array. Other details of the data are closer to the theoretical curves for $p = 0.53$. This may be due to the oversimplification of the true, ramified structure of the regions of missing sites, which in the model are approximated by circular hole. On the other hand, concerning the probability distribution $D(N)$ of these holes the exponent $s = 1.8$, corresponding to the

experimental situation, is more satisfactory than a form for D which would give more weight to large holes.

In section IIIA, equations (36) and (37), we have introduced the notion of a vortex impedance $Z_V = R_V + i\Omega L_V$. At low frequencies its real part is thermally activated as shown in figure 7. This behaviour is confirmed by the measurements presented in ref.¹¹. The slope of the theoretical curves at high enough temperature (e.g., around $t = 5$) yields activation energies of about 4 and 2.6 in unit of J for $p = 0.515$ and $p = 0.53$ respectively, in good agreement with the experimental data. For very low temperatures the curves become flat. However, in between the two limiting regimes there is another common slope in the R_V vs $1/t$ plot at about $1/t = 0.6$ for $p = 0.515$ and $1/t = 1.1$ for $p = 0.53$ in our theoretical plots. The measurements do not really exhibit our second common slope but the curves in ref.¹¹ for 317 Hz and lower frequencies do indeed show a tendency to a steeper slope before they approach the constant value in the low temperature limit. In this respect the experimental data look more similar to our curves for a larger percolation fraction ($p = 0.53$ in figure 7).

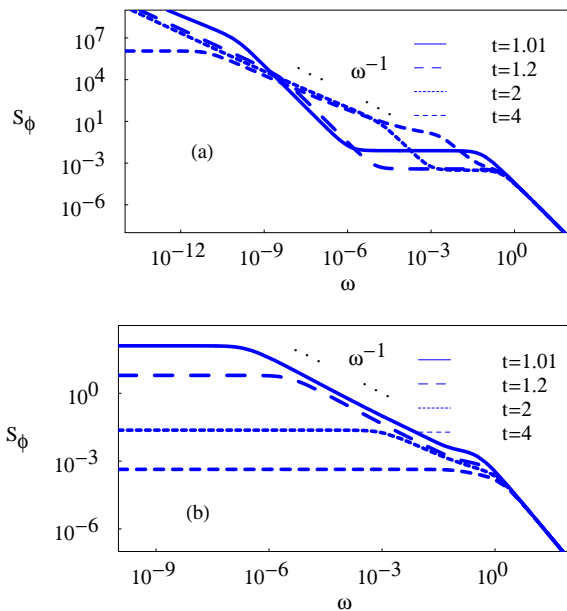


FIG. 8: Flux noise S_ϕ vs ω for (a) $p = 0.515$ and (b) $p = 0.6$. $s = 1.8$.

Finally we present, in figure 8, the flux noise spectrum resulting from our multiple trapping approach, for different temperatures and p . Flux noise is an interesting observable even for regular arrays^{3,19}. It is white (frequency independent) for sufficiently low ω with a value that depends on T . For intermediate frequencies the curves for different T are identical, having a $1/\omega$ slope. This universality has been explained in different ways, for example by invoking the dynamic response of bound

vortex-antivortex pairs which exist below T_{BKT} ,¹⁹ but also above, with a finite life-time. It is interesting to note that disorder seems to produce a similar behaviour, although the intermediate regime has structure superposed on a simple $1/\omega$ dependence, specially for p close to p_c . In particular, there is another white noise region for higher frequency, before the behaviour crosses over to $1/\omega^2$ at high frequencies. This structure is again a consequence of the frequency dependence of the vortex mobility. Moreover, the universality in this regime is not perfect: even for $p = 0.6$ the curves are not on top of each other. Unfortunately there are, at least for the time being, no experimental data to compare with.

V. SUMMARY AND CONCLUSIONS

We have aimed at explaining the electrodynamic response of a Josephson junction array in which a substantial fraction of the superconducting sites is missing. For the motion of thermally excited vortices and antivortices in this type of strongly disordered array we have used a multiple trapping model. The regions of missing sites are grouped into holes which we take to be of circular shape. When a vortex or antivortex reaches a hole it has some probability of being trapped into the hole (pinning effect). It can later on be released due to thermal excitation. The effect of this disorder is phrased in terms of a frequency dependent vortex mobility which determines observable quantities, such as the electrical conductance, composed by the sheet resistance R_s and the inductance L_s of the array, or the flux noise. We find the following results :

(i) R_s exhibits three frequency regimes. At very low and high frequency ω a white spectrum is observed with a much lower value for low ω than for large ω . For the time scale corresponding to the latter regime vortices remain either trapped in a hole or free outside any hole. Thus the mobility, and the corresponding response is given by the one of a regular array. At the opposite end, for very low frequencies, vortices get trapped many times during one excitation cycle, which strongly reduces their mobility. For intermediate frequencies $R_s \propto \omega^x$ with x varying between $x = 1$ and $x = 2$. For higher temperatures the $R_s \propto \omega$ almost coincide, signalling some kind of universality. These features are in good agreement with the experimental data in ¹¹.

(ii) For the inductive part we find $L_s^{-1} \propto \omega^2$ at low ω while for intermediate frequency regime L_s^{-1} is independent of ω . For large frequencies a tendency of L_s^{-1} to grow with frequency with some new exponent is also seen for higher values of p . The critical frequency for crossover from $L_s^{-1} \propto \omega^2$ to constant L_s^{-1} decreases with the decrease of temperature T and percolation fraction p . These results also reproduce well the experimental data of reference¹¹.

(iii) For a given frequency the vortex resistance is thermally activated at sufficiently high temperatures. The

activation energy on the order of 4 times the Josephson coupling between the existing superconducting sites corresponds to the measured value. For lower temperatures a tendency towards another activated form of the R_V versus $1/T$ curves appears, which is also visible as a tendency in the measured data.

(iv) We have also evaluated the frequency dependent flux noise. $1/\omega$ noise is achieved for the intermediate frequencies separating the white noise part for small ω and $1/\omega^2$ noise for very high frequencies. thus the presence of disorder leads to similar results as seen in regular arrays.¹⁹ However at very close to p_c the flux noise data has some unexpected flatening before turing to $1/\omega^2$ part which is a consequence of the frequency dependence of the vortex mobility. Unfortunately there are no experimental flux noise data for the disordered arrays to compare with our theoretical investigations.

Acknowledgments

We thank Piero Martinoli and Philippe Curty for interesting discussions. This work was supported by the Swiss National Science Foundation under the project no. 2000-067853.02/1.

References

- ¹R. S. Newrock, C.J. Lobb, U. Geigenmüller, M. Octavio, Solid State Physics 54, 263 (2000).
- ²P.Martinoli. Ch. Leemann, Journal of Low Temperature Physics 118, 699 (2000).
- ³Md. Ashrafuzzaman and H. Beck, Studies of High Temperature Superconductors (Nova Science, New York, 2002), Vol.43.
- ⁴H. Beck and D. Ariosa, Solid state communications 80, 657 (1991).
- ⁵P.J. Flory, J. Am. Chem. Soc. 63, 3083 (1941).
- ⁶W.H. Stockmayer, J. Chem. Phys. 11, 45 (1943).
- ⁷S. R. Broadbend and J. M. Hammersley, Proc. Camb. Phil. Soc. 53, 629 (1957).
- ⁸B.B. Mandelbrot, The fractal geometry of nature, Freeman, San Francisco (1977).
- ⁹A. Bunde and S. Havlin, Fractal and Disorder Systems, Springer-Verlag, Berlin (1991).
- ¹⁰A.L. Eichenberger, J. Affolter, M. Willemin, M. Mombelli, H. Beck, P. Martinoli, S.E. Korshunov; Phys Rev Lett 77, 3905 (1996).
- ¹¹Jérôme Affolter, PhD thesis, Institute of Physics, University of Neuchatel, Switzerland (2001), and to be published.
- ¹²T. Nakayama, K. Yakubo, R.L. Orbach ; Rev Mod Phys 66, 381 (1994).
- ¹³M. Mombelli, H. Beck ; Phys Rev B57, 14'397 (1998).
- ¹⁴M.P.A. Fisher, Phys Rev Lett 62, 1415 (1989).
- ¹⁵M.V. Feigel'man, V.B. Geshkenbein, A.I. Larkin, V.M. Vinokur; Phys Rev Lett 63, 2303.
- ¹⁶M. Calame, S.E.Korshunov, Ch.Leemann, P.Martinoli; Phys Rev Lett 86, 3630 (2001).
- ¹⁷H. Scher and E.W. Montroll, Phys Rev B12, 2455 (1975).
- ¹⁸Md. Ashrafuzzaman, H. Beck, Journal of Magnetism and Magnetic Materials (JMMM), Vol 272-276P1 pp 284-285.
- ¹⁹Md. Ashrafuzzaman, M. Capezzali and H. Beck, Phys Rev B 68, 052502 (2003).
- ²⁰A. Jonsson and P. Minnhagen, Phys Rev B55, 14 (1997).
- ²¹ Md. Ashrafuzzaman, Ph. Curty, M. Neef and H. Beck, Inst. of Physics, University of Neuchatel, Switzerland (2002), unpublished.